

RESEARCH ARTICLE

10.1002/2017JD027480

Key Points:

- The Uintah Basin of Utah has previously been estimated to have large leakage rates of methane based on a single-aircraft research flight
- This study supports large leak rate estimates by combining in situ ground-based observations with atmospheric modeling
- A recent spatially explicit methane emission inventory from the EPA underestimates methane emissions within the Uintah Basin

Correspondence to:

C. S. Foster,
chris.foster@utah.edu

Citation:

Foster, C. S., Crosman, E. T., Holland, L., Mallia, D. V., Fasoli, B., Bares, R., ... Lin, J. C. (2017). Confirmation of elevated methane emissions in Utah's Uintah Basin with ground-based observations and a high-resolution transport model. *Journal of Geophysical Research: Atmospheres*, 122, 13,026–13,044. <https://doi.org/10.1002/2017JD027480>





Received 20 JUL 2017

Accepted 12 NOV 2017

Accepted article online 15 NOV 2017

Published online 4 DEC 2017

Confirmation of Elevated Methane Emissions in Utah's Uintah Basin With Ground-Based Observations and a High-Resolution Transport Model

C. S. Foster¹ , E. T. Crosman¹ , L. Holland², D. V. Mallia¹, B. Fasoli¹, R. Bares¹, J. Horel¹ , and J. C. Lin¹ 

¹Department of Atmospheric Sciences, University of Utah, Salt Lake City, UT, USA, ²Department of Atmospheric Sciences, University of Hawai'i at Mānoa, Honolulu, HI, USA

Abstract Large CH₄ leak rates have been observed in the Uintah Basin of eastern Utah, an area with over 10,000 active and producing natural gas and oil wells. In this paper, we model CH₄ concentrations at four sites in the Uintah Basin and compare the simulated results to in situ observations at these sites during two spring time periods in 2015 and 2016. These sites include a baseline location (Fruitland), two sites near oil wells (Roosevelt and Castlepeak), and a site near natural gas wells (Horsepool). To interpret these measurements and relate observed CH₄ variations to emissions, we carried out atmospheric simulations using the Stochastic Time-Inverted Lagrangian Transport model driven by meteorological fields simulated by the Weather Research and Forecasting and High Resolution Rapid Refresh models. These simulations were combined with two different emission inventories: (1) aircraft-derived basin-wide emissions allocated spatially using oil and gas well locations, from the National Oceanic and Atmospheric Administration (NOAA), and (2) a bottom-up inventory for the entire U.S., from the Environmental Protection Agency (EPA). At both Horsepool and Castlepeak, the diurnal cycle of modeled CH₄ concentrations was captured using NOAA emission estimates but was underestimated using the EPA inventory. These findings corroborate emission estimates from the NOAA inventory, based on daytime mass balance estimates, and provide additional support for a suggested leak rate from the Uintah Basin that is higher than most other regions with natural gas and oil development.

1. Introduction

The rapid growth of oil and natural gas production infrastructure in the last 15 years through horizontal drilling and hydraulic fracturing has raised concerns regarding pollution of water and the impacts of associated emissions on air quality and climate, primarily through the emissions of methane (CH₄), the main component of natural gas (Brandt et al., 2014; Rozell & Reaven, 2012; Wang et al., 2014). While natural gas has been recognized as a “bridge fuel” to facilitate a “decarbonized energy system” due to lower production of carbon dioxide than other fossil fuels during combustion (Brandt et al., 2014), CH₄ has a high potential as a greenhouse gas (if leaked directly to the atmosphere), and improved understanding of its emissions from anthropogenic activities is necessary (Turner et al., 2016). Thus, a compelling need exists to improve current CH₄ emission estimates associated with natural gas and oil activity to inform leakage and emission mitigation policies such that leakage of CH₄ associated with natural gas production does not offset the potential climate benefits of the transition to a cleaner fuel (Mayfield, Robinson, & Cohon, 2017; Ravikumar & Brandt, 2017).

Both “bottom-up” and “top-down” methods are used to estimate leakage/emission rates of CH₄ and other trace species associated with oil and gas production. Top-down methods use atmospheric observations, mainly aircraft or ground-based, and transport models to constrain emissions in source regions (Karion et al., 2013, 2015; Oltmans et al., 2016; Petron et al., 2014). Through a combination of in situ CH₄ concentrations and meteorological transport modeling, emission rates can be inferred (Turner et al., 2016). In contrast, bottom-up methods account for sector-specific emissions by collecting a database of activity rates specific to the various emitters in the industry, such as production facilities and wells. These activity rates are then multiplied by estimated emission factors (per unit activity) to determine an emission rate (Desai & Harvey, 2017; Maasackers et al., 2016). A combination of surveys on national energy usage data and agricultural activities, along with greenhouse gas emissions data from different sources, are used to estimate emissions of criteria pollutants and greenhouse gases in the U.S. (Bar-Ilan et al., 2008; Lyon et al., 2015; Maasackers et al., 2016; Subramanian et al., 2015). Bottom-up CH₄ inventories have been shown to underestimate national CH₄

emissions by a factor of ~1.2–1.7 nationally and by a factor of ~2.7 in the oil and gas regions of the south central U.S. (Brandt et al., 2014; Miller et al., 2013). In the San Juan Basin of Colorado and New Mexico, CH₄ emissions were found to be unaffected by a sharp decrease in natural gas production, illustrating the complexity of relating production statistics to “pathways” for CH₄ leakage (Smith et al., 2017).

Across the U.S., a number of recent studies have utilized top-down aircraft in situ airborne measurements of methane (CH₄) to estimate both total emission rates from various production regions in addition to the loss rates from shale oil and gas production. Large differences in regional CH₄ loss or “leakage” rates have been noted in the literature (Peischl et al., 2015). Leakage rates from production of natural gas in the Haynesville (Texas/Louisiana), Fayetteville (Arkansas), Marcellus (Pennsylvania), and Barnett (Texas) regions were between 0.18 and 2.8% (Karion et al., 2015; Peischl et al., 2015). Higher CH₄ production loss rates were found in the Bakken production region of South Dakota (4.2%–8.4%) (Peischl et al., 2016) and the Denver-Julesburg Basin in northeastern Colorado (2.6%–5.6%) (Petron et al., 2014). In the Uintah Basin, Karion et al. (2013) estimated a basin-wide emission rate of $55 \times 10^3 \text{ kg h}^{-1}$ using in situ aircraft measurements from mass balance flights on a single day (3 February 2012). Based on production, a corresponding leakage rate of 6.2%–11.7% of the production amount was calculated (Karion et al., 2013). Using the Karion result, Robertson et al. (2017) found that well pads accounted for 36% (19–70%, 1 σ) of total basin-wide emissions, suggesting that emissions from this sector are an important contributor overall. The Uintah Basin is thus thought to be unique in having CH₄ leak rates much higher than those observed in most other basins in the United States. For comparison, the Uintah Basin leakage rates are greater than the comparatively small leakage rates in the Barnett Shale, Texas, region by a factor of 7 (Karion et al., 2015).

Oil and natural gas exploration, production, gathering, processing, and transportation take place in many areas throughout the western United States, including the Uintah Basin in north-eastern Utah (Figure 1). The Basin ranges in elevation from 1,400 m to 1,700 m above sea level (asl), with the surrounding mountains rising to between 2,000 and 3,500 m asl. Over 10,000 producing oil and gas wells currently operate within Basin that contribute ~1% of the total U.S. natural gas. The large, bowl-shaped topography of the Uintah Basin often results in pollutants being trapped within its confines during stable conditions, while a number of other complex meteorological processes also affect transport of emitted species from oil and gas activities (Lyman & Tran, 2015; Neemann et al., 2015).

The Uintah Basin has been the focus of several studies and field campaigns investigating the impacts of oil and natural gas emissions on air quality in the region (e.g., Edwards et al., 2014; Schnell et al., 2009, 2016; Yuan et al., 2016; Zatko et al., 2016). Most recently, the Uintah Basin was the locus of the SONGNEX (Shale Oil and Natural Gas NEXus) airborne field campaign, which took place during the spring of 2015 over multiple oil and gas fields in the U.S. (NOAA, 2014).

This study aims to evaluate recently produced emission inventories to verify their proposed emission rates within the Uintah Basin. Specifically, we examine the robustness of the emission inventory created by Maasackers et al. (2016) and the result from Karion et al. (2013), thereby assessing whether daytime mass balance estimates from aircraft flights are representative of diurnal fluxes in the Uintah Basin. In doing so, we seek to test recent findings that claim the Uintah Basin is unique in its unusually high CH₄ leakage rates. In addition, this study seeks to simulate, for the first time, spatial and diurnal variations in CH₄ within the Basin. We utilize an atmospheric transport modeling framework consisting of meteorological fields from the Weather Research and Forecasting (WRF) and High Resolution Rapid Refresh (HRRR) models and the Stochastic Time-Inverted Lagrangian Transport (STILT) model (Lin et al., 2003; Nehrkorn et al., 2010). We compare these modeling results against a unique observational data set of in situ observations of CH₄ from three sites in the Uintah Basin for a 6 week period from 19 April 2015 to 31 May 2015 during the SONGNEX field campaign. A second period from 19 April 2016 to 31 May 2016 was analyzed to leverage observational data from the temporary measurement site at Castlepeak in the western portion of the Basin in the middle of densely situated oil wells (Figure 1b).

2. Data and Methods

2.1. Study Period

Two 6 week periods are the focus of this study: 19 April to 31 May 2015 and 2016. The 19 April to 31 May 2015 period coincides with the SONGNEX field campaign. The months of April and May are ideal for

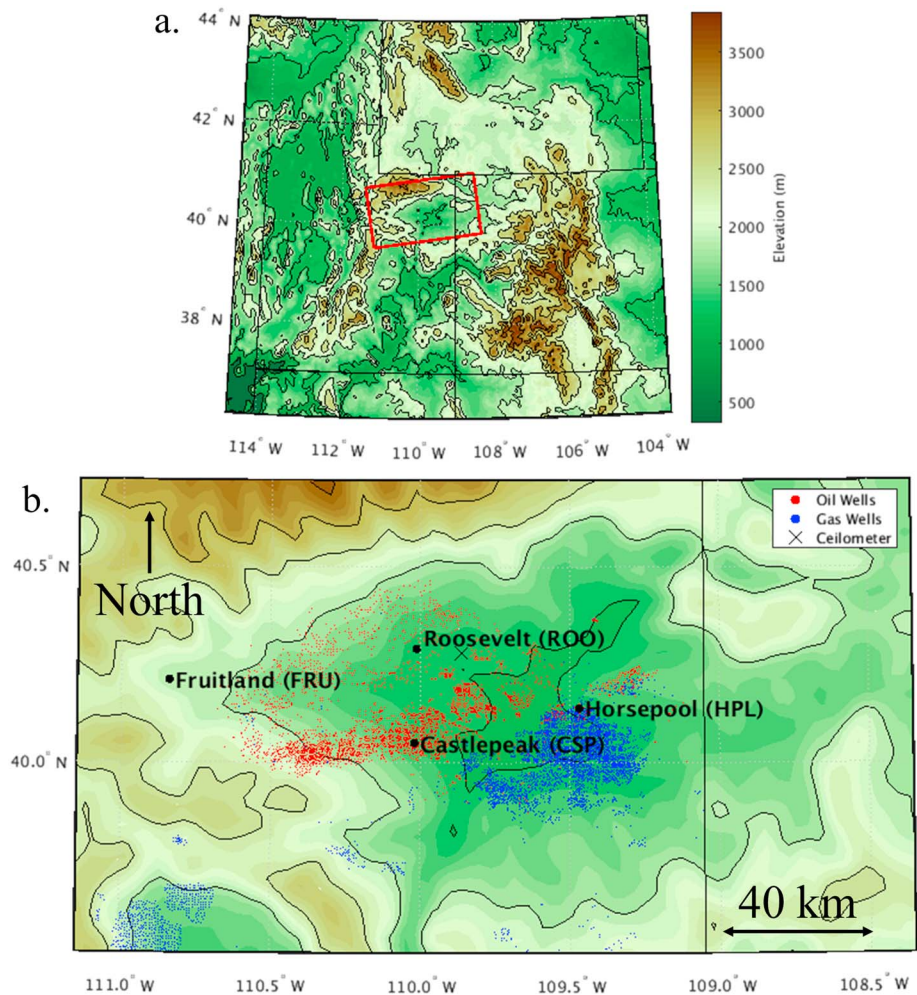


Figure 1. (a) Elevation map (m) of Utah and surrounding states with a red rectangle indicating the location of the Uintah Basin. (b) Elevation map (m) of Uintah Basin showing the location of the Fruitland, Roosevelt, Horsepool, and Castle Peak observing sites. The red dots are active and producing oil well locations. The blue dots are active and producing gas wells. The black "X" indicates the location of a ceilometer referenced in this study.

meteorological and air chemistry modeling purposes; observed solar insolation provides heating adequate to mix-out nocturnal stable layers each morning-afternoon, allowing model errors to be restricted to a single diurnal cycle.

Modeled and observational analyses were conducted on all "quiescent" days during the two 6 week periods. Quiescent days were defined as those days without extensive cloud cover, precipitation, or strong downslope westerly winds, which is a common feature on the western slope of the Basin. Days not meeting these criteria were removed from the final analysis as the WRF model simulations were often unable to properly simulate either strong downslope winds or the placement of mesoscale precipitation bands. These model shortcomings are hypothesized to be due to the inadequate model boundary layer physics observed during turbulent interactions between large-scale winds and near-surface stable layers (Crosmán & Horel, 2017), and the highly localized and terrain-sensitive nature of precipitation bands observed within this region. Thirteen of the 42 days within the study period in 2015 were removed from the analysis due to rainfall (7 and 24–25 May) or downslope winds (27 April and 9–14, 17, 19, and 22 May). In 2016, 13 days were also removed from the analysis due to rainfall (19, 26, and 28 April and 8, 16, and 21 May) and downslope winds (23 and 24 April and 1, 8, 9, 21–22, 24, and 26 May). Once the days with disturbed conditions were removed from the model analysis, 29 quiescent days in 2015 and 2016 remained to compare to those days when observational data were available.

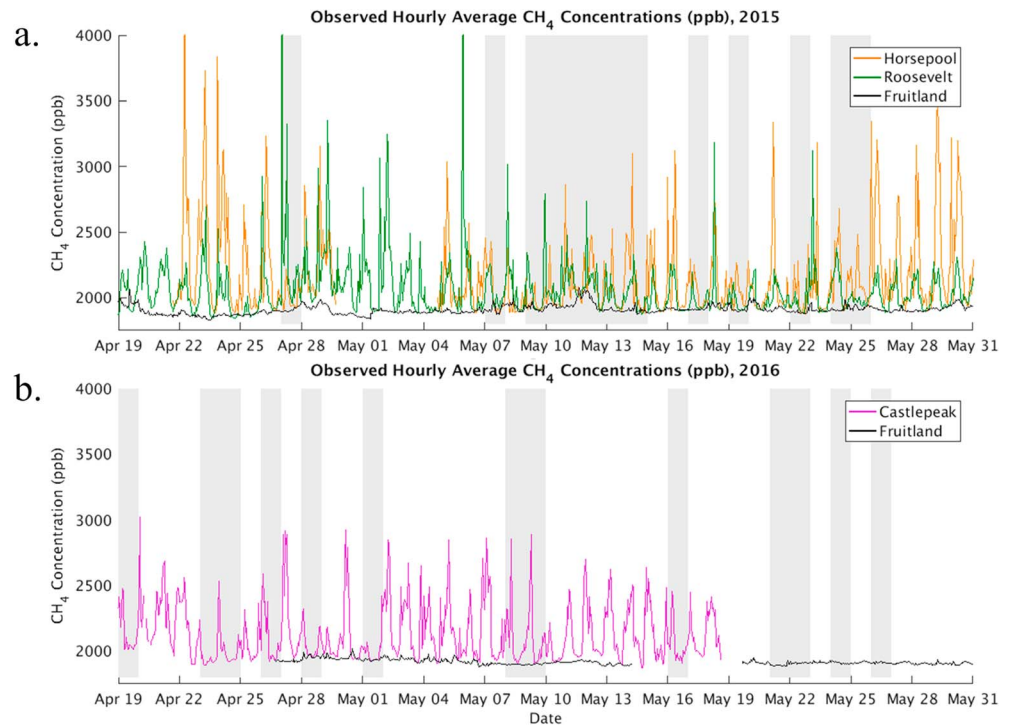


Figure 2. (a) Hourly averaged CH₄ concentrations (ppb) at Horsepool (orange), Roosevelt (green), and Fruitland (black) from 19 April 2015 to 31 May 2015. (b) Hourly averaged CH₄ concentrations (ppb) at Castlepeak (purple) and Fruitland (black) from 19 April 2015 to 31 May 2016. The shaded times are considered nonquiescent and removed from the final analysis. The ticks are marked at 12 a.m. MST every 3 days.

2.2. Observations of CH₄ and Meteorology

High-frequency CH₄, CO₂, and H₂O observations have been collected since January 2015 at three sites within the Uintah Basin: Fruitland (FRU), Roosevelt (ROO), and Horsepool (HPL), by the Utah Atmospheric Trace gas and Air Quality lab at the University of Utah. A fourth site, Castlepeak (CSP), operated from November 2015 to May 2016 (Figure 1b). Each observing site is equipped with a suite of instrumentation measuring meteorological observations and atmospheric trace species. Time series of CH₄ from FRU, HPL, and ROO are shown from 19 April to 31 May 2015 in Figure 2a and for FRU and CSP for the 19 April to 31 May 2016 period in Figure 2b.

Concentrations of CH₄ ($\sigma = \pm 4.5$ ppb), CO₂ ($\sigma = \pm 0.37$ ppm), and H₂O ($\sigma = \pm 61$ ppm) were measured optically using a Los Gatos Research (LGR) Ultraportable Greenhouse Gas Analyzer (model 907–0011, Los Gatos Research Inc, San Jose, Ca.). Measurements from the LGR were collected every 10 s. H₂O mole fractions were calibrated using a Li-Cor LI-610 dew point generator at a 3 month interval. Corrections for water vapor dilution and spectral line broadening on CO₂ and CH₄ were made mathematically by the LGR and validated empirically in laboratory testing. Automated calibrations of CO₂ and CH₄ concentrations were performed every 3 h using three compressed air tanks with known concentrations tertiary to the WMO CO₂ and CH₄ scales and spanning the expected range of observations. To account for instrumentation drift, we linearly interpolated measurements of calibration gases during the sampling periods and used ordinary least squares regression to produce unique correction coefficients for each data point. Real-time and historic measurements from all sites can be viewed at <http://air.utah.edu>.

The FRU site is situated on the western edge of the Uintah Basin at 2,020 m above sea level and is considered the background site (Figure 1b). Since FRU is ~400 m higher than ROO and CSP and upwind of the Basin relative to prevailing synoptic-scale westerlies (see section 3.1), FRU experiences minimal influence from emissions within the Basin during most of the year. During the 19 April to 31 May 2016 periods, CH₄ concentrations at FRU remained below 2.0×10^3 ppb. HPL, located in the south-eastern portion of the Basin, is in an area dominated by the extraction and production of natural gas with active extraction occurring within 200 m of the measurement site. Horsepool has been the observational focus of multiple recent

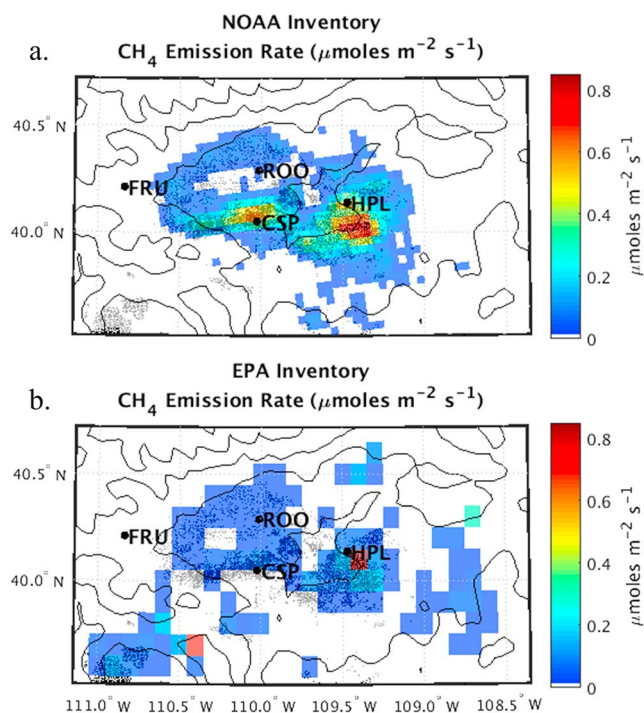


Figure 3. (a) Emission rate of CH₄ ($\mu\text{mol m}^{-2} \text{s}^{-1}$) within the Uintah Basin, Utah, at 4 km resolution from the NOAA inventory (Ahmadov et al., 2015). (b) As in Figure 3a except at 0.1° resolution from the EPA inventory (Maasackers et al., 2016). Oil and gas well locations are shown as light gray dots.

studies examining ozone chemistry within natural gas and oil producing basins, suggesting its prominence as a field-intensive observing site in the region (Ahmadov et al., 2015; Edwards et al., 2014). ROO and CSP are situated in the western portions of the Basin. ROO is at an elevation of 1,585 m above sea level in an urban area with sparsely situated oil wells surrounding the region, whereas CSP (elevation 1,600 m) is found in the west-central portion of the Basin, in an area with dense oil wells.

Meteorological observations (temperature, wind speed, wind direction, and relative humidity) at temporal frequency ranging from 1 to 15 min were obtained from observations carried out by Utah State University, University of Utah, and Division of Air Quality sites at ROO, HPL, and FRU. A Vaisala ceilometer was installed in January 2014 at the Uintah River High School in Fort Duchesne, Utah, which is located at an elevation of 1,540 m in the center of the Basin. Many approaches are used to estimate boundary layer characteristics from ceilometers, and every algorithm has its limitations (Kotthaus et al., 2016). As discussed by Ware et al. (2016), the boundary layer height derived from radiosondes may not always correspond to mixing heights. Our approach for this study used combined visual inspection of daily backscatter imagery (to remove contamination by multiple layers, tenuous clouds, etc.) and best practice backscatter processing techniques that have been developed at the University of Utah over the last 5 years in different basins within Utah (Neemann et al., 2015; Young & Whiteman, 2015). Our technique uses a 24 h rolling period and two-dimensional image thresholding processing techniques (Sahoo, Soltani, & Wong, 1988) to identify gradients and hence layers in the

ceilometer images. The backscatter signal was too weak in the afternoon to derive estimates, so our approach was to limit the use of the ceilometer information to the nighttime to midmorning period. Six rawinsonde launches were conducted at HPL during an intensive observational period on 28 and 29 April 2015.

2.3. CH₄ Emission Inventories

Two recent emission inventories that currently include gridded CH₄ emission rates in the Uintah Basin, Utah, were produced by Ahmadov et al. (2015) and Maasackers et al. (2016) (Figures 3a and 3b). These inventories are used in conjunction with meteorological models and the STILT transport model framework to produce hourly CH₄ concentrations at the measurement locations (ROO, HSP, and CSP).

The methane inventory in the Uintah Basin developed by the National Oceanic and Atmospheric Administration (NOAA) (Ahmadov et al., 2015) (hereafter referred to as the “NOAA” inventory) used the locations of oil and gas wells across the Uintah Basin (see Figure 1b) to spatially allocate the aircraft-derived Basin-wide CH₄ emission rate from Karion et al. (2013) over the area of the Basin and is gridded at 4 km spacing (Figure 3a). The Basin-wide emission rate of $55 \times 10^3 \text{ kg h}^{-1}$ was calculated based on in situ aircraft measurements from mass balance flights from a single day (3 February 2012) (Karion et al., 2013). Figure 3a shows the average CH₄ flux ($\mu\text{mol m}^{-2} \text{s}^{-1}$) estimated within the Uintah Basin based upon the results of the NOAA inventory. An area of high emissions over the central portion of the Basin, south of HPL, corresponds to the highest density of natural gas wells (Figure 1b). Another area of high emission rates near CSP corresponds to a region of dense oil wells. To the north, the CH₄ emission rates are low, which corresponds with an area where oil well density is minimal.

The Maasackers et al. (2016) inventory (hereafter referred to as “Environmental Protection Agency (EPA) inventory”) of U.S. CH₄ emissions is a bottom-up approach based upon the U.S. Environmental Protection Agency’s 2012 inventory of U.S. Greenhouse Gas Emissions and Sinks (GHGI) at a spatial resolution about half that of the NOAA inventory (i.e., grid spacing was roughly two times coarser). The GHGI national data used in the EPA inventory includes individual emission types of natural gas systems, agriculture

Table 1
Summary of WRF Model Characteristics

Parameter	Chosen setup
Initial/boundary conditions	HRRR and NAM analysis
Vertical levels	51 ETA levels
Domains	domain
Resolution	4 km
Time step	18 s
Land surface	USGS
Microphysics	Thompson Graupel Scheme
Planetary boundary layer	Mellor-Yamada-Janjic
Land surface	Unified Noah
Radiation (short and long wave)	RRTMG
Surface layer	Eta similarity
Cumulus	Kain-Fritsch

(e.g., enteric fermentation and rice cultivation), landfills, coal mining, manure management, petroleum systems, and forest fires. The U.S. national emissions reported in the GHGI are spatially disaggregated to 0.1° grid spacing (~8.5 km in the area of interest) and monthly temporal resolution (Maasackers et al., 2016). Where possible, facility-level emission data are used. Figure 3b shows the CH₄ emission rate used in this study, based upon the EPA inventory. The values shown were obtained by upscaling the 2012 EPA emissions to 2015 based on the percentage increase of active and producing natural gas and oil wells in the Uintah Basin (a factor of 12%) and subsequently used in the STILT-based calculations for the EPA inventory. After upscaling, the EPA basin-wide methane emission rate is $31.1 \times 10^3 \text{ kg h}^{-1}$ (summed over the area shown in Figure 3), which is about 45% lower than the NOAA emission inventory ($56.5 \times 10^3 \text{ kg h}^{-1}$).

2.4. WRF/HRRR and STILT Modeling

Two meteorological model data sets are utilized. We ran the Weather Research and Forecasting model (WRF) version 3.4 (Skamarock et al., 2008), from 18 April to 31 May 2015. In addition, model output from the National Centers for Environmental Prediction High Resolution Rapid Refresh (HRRR) model analyses archived by the NOAA Air Resources Laboratory was also obtained for the period from 18 April to 31 May 2016.

WRF was configured for the 2015 simulation period based upon a separate STILT study focusing on the Salt Lake City area, also in Utah (Mallia et al., 2015), and was recompiled to allow for time-averaged, mass coupled winds for driving STILT (Nehrkorn et al., 2010). The 2015 WRF model configuration (see Table 1 for summary of WRF settings) consisted of a 4 km domain centered over the Uintah Basin, encompassing all of Utah and parts of surrounding states (Figure 1a). Initial and boundary meteorological conditions were obtained from the HRRR model analysis obtained from the NOAA National Operational Model Archive and Distribution System when available (Benjamin et al., 2016), and the North American Mesoscale model (NAM) during a one-week period when HRRR analysis was not available. Boundary conditions were derived from either HRRR (every 1~2 h) or NAM (every 6 h), depending on data availability. Table 2 outlines these periods as well as the initial/boundary conditions applied during each WRF model simulation. WRF model simulations in 2015 were initialized once a week over the period. Each 7 day simulation was preceded by a 6 h spin-up period. The Thompson microphysical scheme and Mellor-Yamada-Janjic planetary boundary layer scheme were used in the simulations based upon the results of previous simulations in Utah basins (Foster et al., 2017; Neemann et al., 2015). Further details of the WRF model setup are given in Table 1.

HRRR model analyses archived by NOAA Air Resources Laboratory are used in this study for the 2016 period. (The HRRR analyses formatted for use directly with STILT were not available for summer 2015.) The HRRR operational model uses the WRF modeling system combined with observational data assimilation and is run over the contiguous U.S. at 3 km resolution (Benjamin et al., 2016). Details on the HRRR model setup are given by Benjamin et al. (2016), with updated information available at <https://rapidrefresh.noaa.gov/>. HRRR incorporates sophisticated data assimilation and has been shown to adequately capture complex up-valley, down-valley, and upslope and downslope thermally driven flows (hereafter referred to collectively

Table 2
Summary of Initial and Boundary Conditions

Begin date	End date	Initial and boundary conditions	Resolution of boundary conditions
18 April 2015, 0000 Z	25 April 2015, 0000 Z	HRRR	1 h
25 April 2015, 0000 Z	2 May 2015, 0000 Z	HRRR	1 h
2 May 2015, 0000 Z	9 May 2015, 0000 Z	NAM	6 h
9 May 2015, 0000 Z	16 May 2015, 0000 Z	HRRR	2 h
16 May 2015, 0000 Z	23 May 2015, 0000 Z	HRRR	2 h
23 May 2015, 0000 Z	31 May 2015, 2300 Z	HRRR	2 h

Note. Spin-up period of 6 h removed.

within the text as “local” or “terrain flows”) within the complex topography of northern Utah (Blaylock, Horel, & Crosman, 2017).

STILT is a particle dispersion model (Lin et al., 2003; Nehrkorn et al., 2010) that uses wind fields provided by WRF and HRRR to drive the backward trajectories. The STILT framework seeks to link atmospheric concentrations at target sites (“receptors”) with upwind source regions at high spatiotemporal resolution (Lin et al., 2003). STILT’s Lagrangian framework is also less dispersive and better at conserving mass than other commonly used Eulerian tracer techniques (Lin et al., 2003; Mallia et al., 2015). One STILT particle represents a parcel of air that is small enough to retain the properties of the surrounding air but large enough that the parcel’s size is larger than the average distance between molecules (Lin et al., 2003). A large number of particles are necessary to fully represent atmospheric transport, while computational resources limit the size of the ensemble that can be simulated (Mallia et al., 2015). In this study, STILT releases 1,000 stochastic particles every hour from the three receptors of interest (HPL, ROO, and CSP) and traces their trajectories backward in time for 24 h.

The STILT-produced backward trajectories are used to calculate footprints—the sensitivity of concentrations at the receptor due to upwind surface influences at each 0.01° grid box (ppm ($\mu\text{mol m}^{-2} \text{s}^{-1}$)⁻¹). More specifically, surface flux footprints $f(x_r, t_r | x_i, y_j, t_m)$ for a given receptor located at x_r at time t_r from an upwind source at (x_i, y_j) and past time t_m are a function of the number of Lagrangian particles residing in the planetary boundary layer (PBL) for that upwind location as given by the equation below:

$$f(x_r, t_r | x_i, y_j, t_m) = \frac{m_{\text{air}}}{h\bar{\rho}(x_i, y_j, t_m)} \frac{1}{N_{\text{tot}}} \sum_{p=1}^{N_{\text{tot}}} \Delta t_{p,i,j,k}$$

where m_{air} is the molecular weight of air, h is the height of the volume in which the surface fluxes are diluted over, $\bar{\rho}$ is the average density of all particles, N_{tot} is the total number of particles, and $\Delta t_{p,i,j,k}$ is the amount of time a particle p spends within the volume at location (x_i, y_j) and time t_m (Lin et al., 2003; Mallia et al., 2015).

For each hour of the study period, footprints derived from the backward trajectories are spatially summed to calculate the time-integrated footprint for each receptor (a 24 h summation of the total influence of the surrounding upwind area). By multiplying the time-integrated footprints with CH₄ emission estimates from emission inventories (converted to units of $\mu\text{mol m}^{-2} \text{s}^{-1}$), an effective contribution toward CH₄ enhancements at the receptor from each grid cell is derived. These CH₄ contributions are then summed over both the x (east-west) and y (north-south) dimensions to calculate a single hourly CH₄ concentration enhancement above the background (ppm) at each receptor. The CH₄ concentration enhancements are then added to the “background” (see discussion below) to derive a simulated CH₄ concentration value for each hour.

Observed CH₄ from FRU (Figure 1b) served as the background or effectively the baseline CH₄ to which STILT-modeled CH₄ enhancements were added. Figure 2 shows the average hourly concentrations of CH₄ at the observing sites. Concentrations at FRU (black line) were nearly always below those observed at the three other sites within the Uintah Basin with minimal diurnal variability (see section 3.1 for the meteorological controls that facilitate its use as a background site).

In the next section, simulated CH₄ concentrations were compared to observed values in an effort to evaluate the veracity of Uinta Basin-based emission inventories estimated in previous studies (Ahmadov et al., 2015; Karion et al., 2013; Maasackers et al., 2016).

3. Results

3.1. WRF Meteorological Model Surface Performance

WRF meteorological simulations were compared against observations at three locations: HPL, ROO, and FRU. The model biases (model-observation) and root-mean-square error (RMSE) for 2 m temperature and 10 m horizontal wind components (u , v), both of which are important variables for assessing WRF model and STILT backward trajectory performance, were calculated as average statistics over the 18 April to 31 May 2015 period. WRF simulations from this study exhibit comparable or better performance than other recent mesoscale simulations conducted in this region, and our error statistics in most cases meet acceptable model benchmarks for complex terrain (Table 3).

Table 3
 Root-Mean-Square Error and Model Bias of Temperature ($^{\circ}\text{C}$), Wind Speed (m s^{-1}), u Wind Component (m s^{-1}), and v Wind Component (m s^{-1}) for FRU, HPL, and ROO

	Temp ($^{\circ}\text{C}$)	Wind speed (m s^{-1})	u wind (m s^{-1})	v wind (m s^{-1})
RMSE				
Fruitland	3.25	2.49	3.68	2.48
Horsepool	2.32	2.16	2.63	2.51
Roosevelt	2.56	2.26	3.32	2.82
Bias				
Fruitland	1.77	0.96	1.69	-0.19
Horsepool	1.18	1.25	0.45	0.36
Roosevelt	0.90	0.93	0.60	-0.02

Generally, the WRF model simulated the wind speed intensity and direction with adequacy at both ROO and HPL. The u and v modeled wind speed biases at ROO and HPL were small, ranging from -0.2 to 0.60 m s^{-1} (Table 3). The RMSE for the simulated u and v wind components at HPL were 2.63 m s^{-1} and 2.51 m s^{-1} , respectively. At ROO, slightly higher RMSE for the u and v wind components were noted (3.32 m s^{-1} and 2.82 m s^{-1} , respectively). At HPL, WRF realistically simulated the nocturnal downslope flows, although there was an eastward bias, possibly due to the terrain resolution in the model (Figure 4b). During the daytime, the timing of observed south-easterly up-valley flow is also well captured by the WRF model, although the wind speed is underestimated during the morning and overestimated in the afternoon. At ROO, WRF simulated the local diurnal wind reversals, although the wind speed is often overestimated (Figure 4a).

The exposure of FRU on the western slope of the Basin to the prevailing westerly flow and its higher elevation ($\sim 400\text{--}500 \text{ m}$) above the Basin floor makes it an ideal location to sample background CH_4 concentrations upstream of the oil and gas emissions. The WRF model's inadequate resolution of small-scale terrain features results in an overprediction of boundary layer terrain-channeled flows (Foster et al., 2017) at this location, resulting in a positive u wind bias of 1.69 m s^{-1} (Figure 4c). The high u wind biases also contributed to the large RMSE for the u wind component (3.68 m s^{-1}). However, the lower model skill at FRU does not affect the use of the FRU CH_4 observations as the background concentrations (section 2.4). Furthermore, these

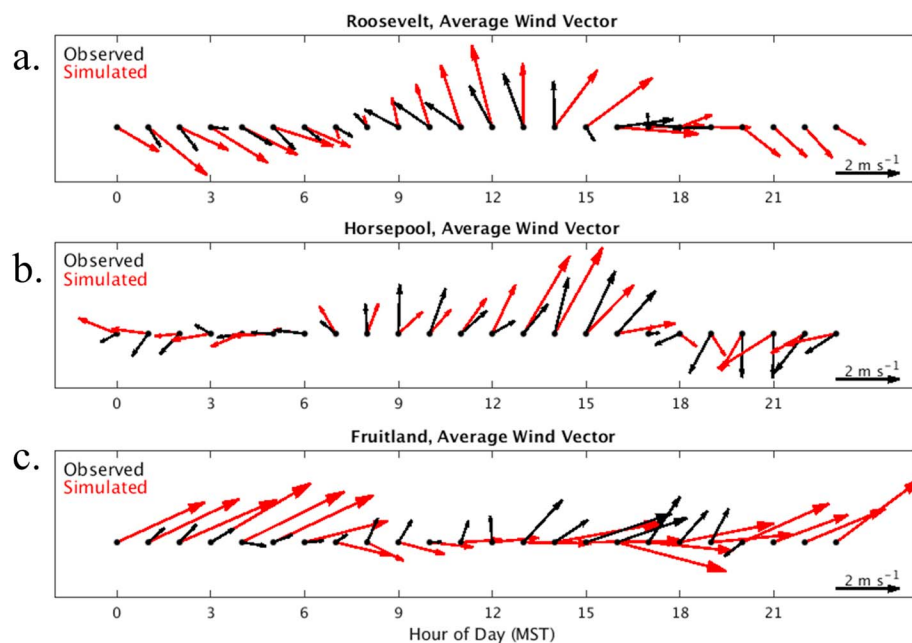


Figure 4. Diurnal variations in average wind vectors on quiescent days at (a) Roosevelt, (b) Horsepool, and (c) Fruitland. The black indicates observation; the red represents simulation. The length of the arrow in the bottom right corner of each panel is equivalent to 2 m s^{-1} .

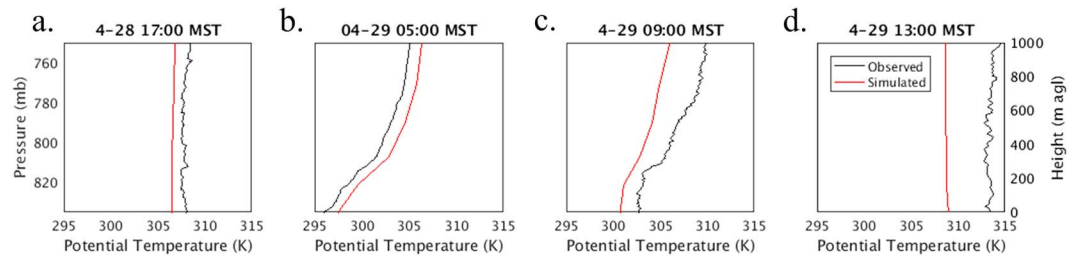


Figure 5. Potential temperature profiles (K) from observation (black lines) and simulation (red lines) at Horsepool. Corresponding time shown above each plot.

strong westerly flows did not penetrate far enough into the Uintah Basin on quiescent days to impact transport calculations.

In terms of WRF model-simulated 2 m temperature, consistent but small WRF model positive biases ($<1.0^{\circ}\text{C}$) at HPL and ROO were noted during 19 April to 31 May 2015, presumably due to inaccuracies in the land cover characteristics, with modeled temperature RMSE at ROO and HPL of 2.32 and 2.56 $^{\circ}\text{C}$, respectively (Table 3). At FRU, the overprediction of terrain-channeled flows contributed to an overestimation in modeled temperatures (positive 1.77 $^{\circ}\text{C}$ bias) due to downslope warming and decreased nocturnal surface cooling associated with the westerly flow.

Model errors for wind and 2 m temperature in other recent modeling studies in the Uintah Basin and Salt Lake Valley of northern Utah were similar or larger than those in this study. For example, a meteorological modeling study conducted by AECOM, Inc. over the Uintah Basin found an overall wind speed RMSE of 2.11 m s^{-1} and a bias of -0.19 m s^{-1} for simulations between March and May at two meteorological sites within the Basin. Another WRF-based study centered on Utah's Salt Lake Valley reported average RMSE for the u and v wind components for 10 WRF model configurations of between 2.67 and 4.0 m s^{-1} , with biases ranging between -1.11 and 1.06 m s^{-1} (Mallia et al., 2015). For 2 m temperature, Mallia et al. (2015) found RMSE in the Salt Lake Valley to range between 1.63 and 2.39 $^{\circ}\text{C}$, with biases of -0.81 to 0.31 $^{\circ}\text{C}$. In a WRF modeling study of a February 2013 cold-air pool in the Uintah Basin, WRF model 2 m temperature RMSE (biases) of 2.98–3.97 $^{\circ}\text{C}$ (0.11–1.65 $^{\circ}\text{C}$) were noted (Neemann et al., 2015).

3.2. Analysis of WRF Simulated Boundary-Layer

Atmospheric soundings are limited in the Uintah Basin as no routine rawinsondes are launched in the area. However, for this study, six research rawinsondes were launched by the University of Utah team on 28 and 29 April 2015 near HPL. Four of these soundings are shown in Figure 5, each highlighting the vertical temperature structure at different times of the day. A deeply mixed daytime PBL extending above 1,000 m above ground level (agl) is evident in both the observation and the simulation during the evening of 28 April and the afternoon of 29 April (Figures 5a and 5d). Toward the end of the night (05:00 MST) the WRF model simulation of the nocturnal inversion extending between the surface and ~ 500 m agl agrees well with observations (Figure 5b). By midmorning (09:00 MST), solar heating begins to erode the residual nocturnal stable layer, resulting in the development of a 400 m deep convective mixed layer near the surface (Figure 5c). Simulated potential temperature profiles capture this deepening morning mixed layer and slight increase in stability within 150 m of the observations, although the strength of the capping inversion was weaker in the simulation than in the sounding. In the afternoon hours, a well-established deep daytime PBL that extends above 1,000 m agl is observed (Figure 5d). WRF-simulated vertical temperature profiles in the PBL had a 1–2 $^{\circ}\text{C}$ positive bias during the late-night hours, and a 2–3 $^{\circ}\text{C}$ negative bias at other times, but because these biases are relatively constant with height, they do not notably impact the evolution of the stability profile of the simulated PBL, as shown in Figures 5b and 5c.

The diurnal variability of the PBL depth (z_i) is associated with large diurnal variations in surface CH_4 concentrations. Because the daytime convective boundary layer and the nighttime stable layer control the vertical extent of dilution of surface emissions (Gerbig, Körner, & Lin, 2008; Seibert et al., 2000), modeled CH_4 concentrations generally increase at night when z_i is low and decrease during the day when z_i increases through convective turbulence. An average diurnal cycle in WRF's simulated potential temperature (θ) profile and the

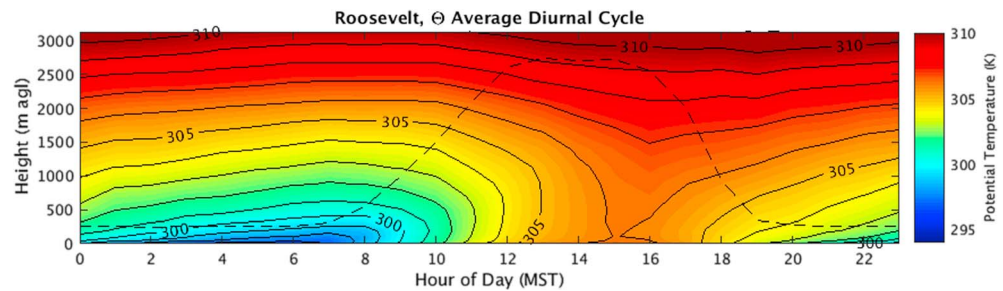


Figure 6. Diurnal average of simulated vertical potential temperature profile (K, shaded and contoured) from 1,500 to 3,500 m asl at Roosevelt (ROO) for quiescent days. Potential temperature is contoured in black every 1 K and labeled every 5 K. The dashed lines represented the average boundary layer height derived from the STILT model.

derived STILT model z_i are shown in Figure 6. The θ profile characteristic of nocturnal stable PBL begins to form shortly after sunset, slowly building into a nocturnal cold-air pool overnight. In the morning, a near-surface mixed layer forms shortly after sunrise, around 0800 MST, and deepens through the midday period. By midafternoon (1300 MST), a deep mixed layer extending over 1,000 m in depth is shown. This overall evolution of z_i agrees with the sounding profiles discussed previously.

An estimate of pollution depth derived from ceilometers is used as a proxy for observed mixing height during nocturnal conditions on a subset of the days analyzed. The z_i for STILT was computed using a modified Richardson method (Vogelezang & Holtslag, 1996) based on meteorological fields from either WRF or HRRR, with a minimum z_i prescribed within STILT at 250 m. Comparison of STILT-derived z_i compared to ceilometer pollution depth (a reasonable proxy estimate for observed z_i) show that STILT-simulated z_i during the night generally agree with observations, with approximately an ~ 60 m shallow bias in STILT (not shown). Ignoring horizontal transport, an uncertainty of ~ 50 – 100 m in z_i during the night would result in an uncertainty of 19–38% in simulated CH_4 , assuming a mean nighttime PBL depth of 250 m. The daytime PBL is deep in both the model and observations (Figures 5a and 5d), and therefore, the sensitivity of simulated CH_4 to these variations is reduced compared to the nighttime case. Since ceilometer aerosol backscatter returns are weak in the afternoon, comparisons between modeled and observed z_i are limited here to the two rawinsonde profiles. The nocturnal ceilometer observations in concert with the rawinsondes shown in Figure 5 provide confidence regarding the realism of the model diurnal PBL evolution and the resulting CH_4 transport and diurnal variability.

3.3. Uintah Basin Meteorological Processes and Observed CH_4 Temporal Variability

Variations in z_i , associated convective vertical mixing, and slope and valley flows are the dominant vertical and horizontal transport mechanisms in the Uintah Basin during the quiescent weather patterns studied here. On quiescent days, the large-scale flow at the 700 hPa level above the surrounding mountains is relatively weak at 5 – 15 m s^{-1} , and transport patterns are dominated by local terrain flows. While wintertime terrain flows in other valleys around Utah have been studied (Foster et al., 2017; Neemann et al., 2015), springtime local flow patterns in the Uintah Basin have not been previously investigated. The STILT model, coupled to meteorological models, provides insight into the impact of these local flows on CH_4 transport and spatial variability within the Basin.

Solar insolation adequate to completely mix-out the stable PBL during the midafternoon is observed on most days during this time of year. An analysis of 24 h backward trajectories at HPL during 2015 found that during each period, more than 99.5% of the 1,000 stochastic particles were transported to the periphery of the Uintah Basin within 24 h. However, nights are long enough to result in moderately intense nocturnal stable boundary layers. This allows for significant buildup of CH_4 each night before mix-out to levels slightly elevated compared to background CH_4 concentrations each afternoon. The observed diurnal cycle of CH_4 at each site during this time is a direct result of the superposition of local flows and z_i evolution.

The imprint of meteorological processes on in situ CH_4 observations at the four sites can be seen in Figures 2a and 2b. The baseline site (FRU) at the western edge of the Basin observes mean diurnal variations in CH_4 of approximately 17 ppb. The extremely small nocturnal increase is only a few percent of the diurnal signals

observed at the low-elevation Basin locations (section 3.5) as a result of the prevailing westerly flow in the FRU region (section 3.1) and its higher elevation that limits transport from the lower elevations of the Basin toward FRU at night (section 3.1). FRU is therefore an ideal location for obtaining upstream background CH_4 concentration for use in the STILT simulations (section 2.4). However, the other three sites experienced considerable day-to-day variability in observed CH_4 concentrations (Figures 2a and 2b). The days with rainfall and stronger downslope winds that were not included in this study analysis tended to have smaller CH_4 enhancements due to the enhanced mixing with the large-scale flow and precipitation (shaded days in Figures 2a and 2b). On the quiescent days when transport was dominated by nocturnal cold-air pools and local flows, CH_4 concentrations rose above 3×10^3 ppb for prolonged nocturnal and morning periods on most days at HPL and CSP (Figures 1 and 2). At ROO, the observed peaks in CH_4 were shorter in duration and more infrequent than at either CSP or HPL. As will be discussed below, contamination by a local source was determined to be impacting the ROO CH_4 observations.

3.4. Observed CH_4 Transport

The transport of CH_4 from local and regional emission sources to the ROO and CSP locations is observed to vary as a function of time of day, wind direction, and wind speed (Figure 7). The three time periods shown in Figure 7 were chosen to highlight key features in the diurnal variation of CH_4 at each of the sites: (1) 22:00–01:00 MST is the transition period between lower concentrations during the day and higher concentrations during the night and the associated flow regimes; (2) 06:00–09:00 MST and (3) 12:00–15:00 MST were selected to show the flow associated with the highest and lowest (respectively) concentrations of CH_4 at the sites. These plots are used to analyze how wind speed and direction impact CH_4 concentrations observed at the three sites. These results can then be related to local features, such as the location of natural gas and oil wells relative to the sites or terrain features that can act to channel flows or influence diurnal slope flows. The influence of the diurnal cycle of atmospheric z_i on CH_4 concentrations is clearly evident in these plots as well, shown by the relative concentrations during each time period (highest in the morning, lowest in the afternoon).

The HPL site is located to the north of and at a slightly higher elevation than many of the gas wells clustered to the south (Figure 1b). During the early evening, winds at HSP are north-easterly, due to downslope flows (slightly higher terrain is noted to the northeast) (Figure 4b). Later in the night, a larger-scale but weak downslope flow develops across the eastern slope of the Uintah Basin, with easterly winds noted until near sunrise (~07:00 MST). After sunrise, the winds shift to southerly with an upslope component, as the Sun heats the elevated slopes to the north of HPL. Between 06:00 and 09:00 MST, the combination of a stable capping inversion above a shallow mixed layer (e.g., Figure 5c) combined with $1\text{--}2 \text{ m s}^{-1}$ upslope flows (Figure 4b) and the cluster of CH_4 emissions from the dense network of gas wells to the south (Figure 1b) results in the highest average CH_4 concentrations at HPL (Figure 7h). In the afternoon, the southerly upslope flow continues, but the deep daytime convective mixing and associated high z_i (e.g., Figure 5d) result in more extensive dilution and lower concentrations in CH_4 being transported to HPL (Figure 7i).

The CSP site is surrounded by a dense network of oil wells on an elevated plateau in the southwestern quadrant of the Basin (Figure 1b). The centralized location of CSP with respect to oil well locations and CH_4 emissions (Figure 3) results in weak sensitivity of the observed CH_4 to wind direction (Figures 7d–7f). The highest CH_4 concentrations are typically associated with very light wind speeds ($0\text{--}4 \text{ m s}^{-1}$). As expected, these maximum CH_4 values are found at night and in the early morning, when the PBL remains stable and when z_i is low.

At ROO the interpretation of the impact of transport patterns and time of day on CH_4 is complicated by a local CH_4 source. Evaluation of the observed time series of CH_4 , mobile field CH_4 observations, and infrared camera imagery of gaseous leakage from storage tanks on the well pad strongly suggests that a nearby oil well is a distinct local CH_4 source that impacts observed concentrations. Careful analysis is required at ROO because this local source is within 150 m distance (and roughly 20 m lower in elevation) from the observation site and is not included in either of the NOAA or EPA emission inventories. This is both a result of the inventories' spatial resolution, which is at a scale of several kilometers (Figures 3a and 3b), and the inability of the inventory methodology to capture local-scale influences. On average, the highest CH_4 concentrations at ROO are observed from sunrise through midmorning (Figure 7b), with an easterly component evident, possibly influenced by the local well. During the afternoon (Figure 7c), concentrations generally decrease to roughly

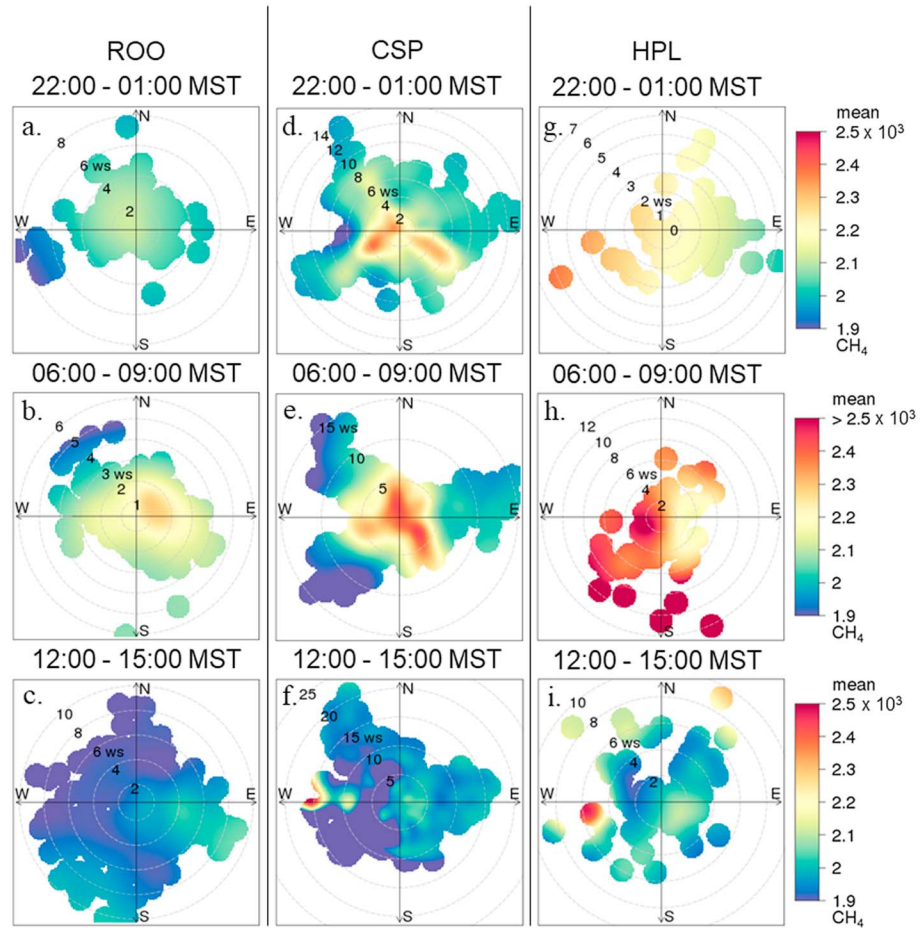


Figure 7. Polar plots showing average CH₄ concentrations (shaded, ppb) given a concurrent wind speed (distance from origin) and direction (location relative to cardinal directions) at Roosevelt from (a) 22:00–01:00 MST. (b) As in Figure 7a except from 06:00 to 09:00 MST. (c) As in Figure 7a except from 12:00 to 15:00 MST. (d–f) As in Figures 7a–7c except for Castelpeak. (g–i) As in Figures 7a–7c except for Horsepool. Time ranges are inclusive.

1.9×10^3 ppb (background). However, when the wind direction is from the east-southeast, directly in line with the nearby oil well, CH₄ concentrations are elevated. During the middle of the night, a down-valley flow originating from the north and west dominates the transport pattern at ROO (Figure 4a), limiting the impact of the nearby local CH₄ source on the observed CH₄ concentrations, which are lower at this time (Figure 7a).

The intermittent “plume-like” nature of the observations at ROO during periods of east-southeast up-valley flow is evident as well by sudden increases in CH₄ as the local plume impacts the observing site, followed by sudden decreases in CH₄ when the local emission plume is no longer impacting the site. For example, during the period shown in Figure 8a, winds start from a north-westerly direction, then shift to an east-southeasterly direction, before returning to the previous regime. Simultaneously, CH₄ concentrations begin at roughly 2×10^3 ppb, then increase intermittently during the period of east-southeasterly down-valley flow to upward of 1×10^4 ppb, and finally decrease to 2×10^3 ppb after a shift back to westerly flow (Figure 8b). As shown in Figure 8b, the standard deviation of CH₄ computed within 10 min of each observation at ROO increases whenever flow is impinging on the site from the southeast. Hence, all observation periods when standard deviations $>0.45 \times 10^3$ ppb were removed from the ROO analysis since they reflect the local emission source rather than the broader impact of the surrounding oil and gas fields.

3.5. STILT-Modeled CH₄ Source Contributions

Three observation sites in the basin (ROO, HPL, and CSP) were used as receptor sites within the STILT modeling framework. The 19 April to 31 May 2015 period was analyzed for CH₄ contributions at ROO and HPL, while

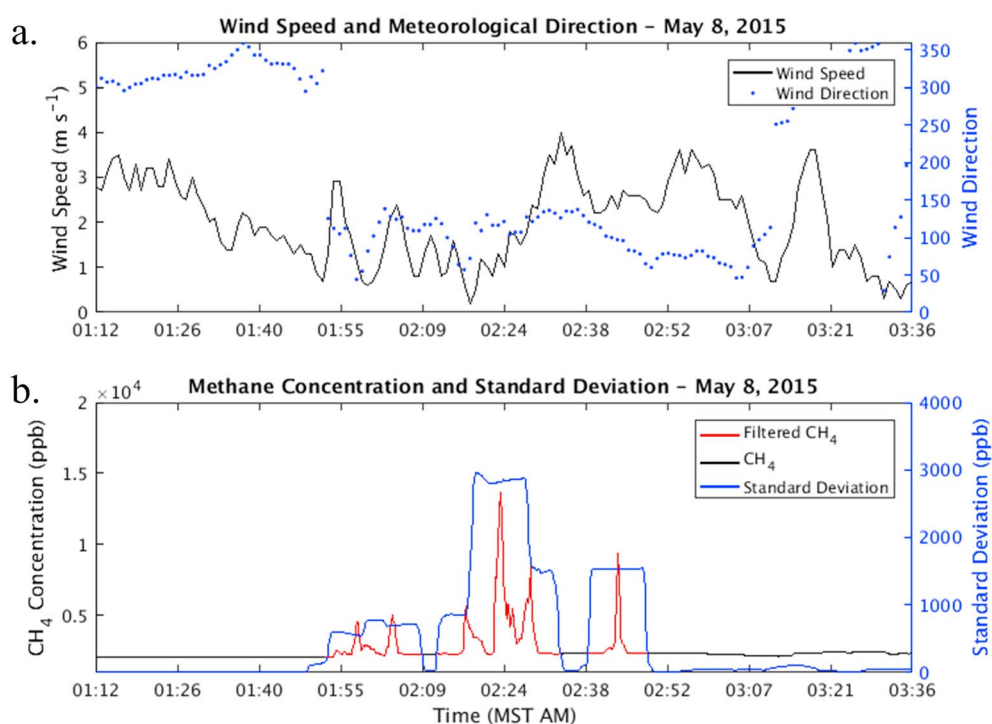


Figure 8. (a) Time series of wind speed (m s^{-1} , solid black line) and direction (blue dots) at Roosevelt from 8 May 2015 01:12 to 03:36 MST. (b) Time series of CH_4 concentration (ppb, solid black and red line) and standard deviation (ppb, solid blue line) from 8 May 2015 01:12 to 03:36 MST. The red sections of the black trace represent CH_4 observations filtered out of the analysis by the standard deviation method.

the 19 April to 31 May 2016 period was analyzed for CH_4 contributions at CSP. The CH_4 emission rate for the entire Uintah Basin was $56.5 \times 10^3 \text{ kg h}^{-1}$ for the NOAA emission inventory and $31.1 \times 10^3 \text{ kg h}^{-1}$ for the EPA emission inventory (Figures 3a and 3b). The majority of emissions in the NOAA emission inventory occur in the regions of dense gas and oil wells (Figures 1b and 3a), simply a result of its methodology of spatially allocating emissions based on well density. Compared to NOAA, the EPA emission inventory has overall lower emissions, with dramatically reduced emissions in the dense oil well region in the western portion of the Basin, and somewhat higher emissions on the eastern slope (Figures 1b and 3b).

STILT simulations were carried out to determine which sectors of the Basin's emission sources impacted the modeled CH_4 concentrations at ROO, HPL, and CSP (Figure 9). The spatial distribution of CH_4 contribution on quiescent days show that most of the CH_4 enhancements at CSP come from the surrounding dense region of oil wells, with slight westerly enhancement potentially explained by an extension of wells located to the west and stronger westerly flows. Most of the CH_4 enhancements at HPL originate from the dense network of gas wells located over a broad region to the south. As discussed previously, transport of CH_4 by upslope flows shortly after sunrise contribute to the CH_4 contributions at HPL being dominated by gas wells within 10 km to the south. At ROO, the prevailing simulated wind direction at night is from the northwest (Figure 4a), resulting in the small simulated CH_4 enhancements at that location originating from scattered oil wells in that region. The light wind speeds (generally $1\text{--}3 \text{ m s}^{-1}$) and the localized nature of terrain flows in different portions of the Uintah Basin result in minimal CH_4 contributions at HPL originating in the oil wells of the western Basin, or CH_4 contributions at CSP originating from the gas wells in the central Basin. Nighttime northeasterly down-valley flows simulated at ROO minimized the emissions that originate from the concentrated oil and gas CH_4 emission regions 20–50 km south and east of ROO. The CH_4 contributions at all three locations were lower for the EPA inventory than for the NOAA inventory, with the largest discrepancy noted at CSP.

3.6. Comparisons Between Modeled Versus Observed CH_4

Modeled and observed concentrations of CH_4 at all receptor sites varied on both temporal and spatial scales, driven by both the meteorology and CH_4 emissions. The modeled average diurnal cycle of CH_4 concentrations

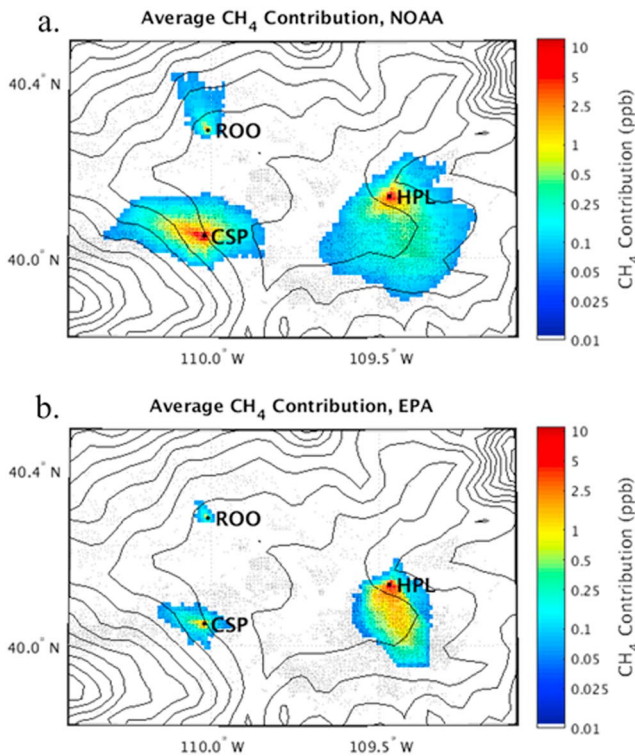


Figure 9. (a) Average CH₄ contribution on quiescent days (shaded, ppb) during the period 19 April 2015 to 31 May 2015 for Roosevelt (ROO) and Horsepool (HPL) using the NOAA emission inventory. For CSP, the average CH₄ contribution is also from quiescent days (shaded, ppb) but during the following year's springtime period (19 April 2015 to 31 May 2016). Elevation contoured as solid black lines every 100 m. (b) As in Figure 9a except for the EPA emission inventory.

(Figure 10) illustrates the sensitivity of the modeled CH₄ enhancements to the large differences in the underlying emission inventories.

The patterns of observed and simulated CH₄ are strongly modulated by the diurnal cycle in convective mixing and associated z_i , as well as variations in the local flows. Commonly, a shallow nocturnal stable PBL is followed by a deep daytime mixed layer, and daytime upslope winds are followed by nighttime downslope winds. The differences between modeled CH₄ concentrations utilizing the NOAA versus EPA inventories were found to be largest during the stable nocturnal period (Figure 10), occurring near 8 a.m. MST (roughly 2.5 versus 2.4×10^3 ppb at HPL and 2.4 versus 2.0×10^3 ppb at CSP). These differences were found to be minimum during the afternoon, when z_i was at its highest, with both inventories producing CH₄ concentrations of roughly 2×10^3 ppb at 6 pm MST.

The observed concentrations of CH₄ and those simulated using the NOAA inventory at CSP increase earlier in the night than at HPL (Figures 10b and 10c). In addition, the increase in the average simulated and observed CH₄ concentrations during the latter half of the night—between 00:00 and 06:00 MST—is ~200 ppb at CSP, but increases by ~400 ppb at HPL. The explanation for these differences is related to local flows and the relative location of the emission sources at these two receptor sites. At CSP, all wind directions result in an accumulation of the CH₄ in the nocturnal PBL as the location is surrounded by oil wells (Figure 1b). However, at HPL, the prevailing downslope north-easterly flows originate from a source region that has few gas wells. Around sunrise, the winds shift to southerly, resulting in the sudden increase in CH₄ as these flows transport CH₄ from the extensive region of gas wells immediately south of HPL (Figure 10b).

The agreement between the simulated and observed diurnal cycle of CH₄ is less at ROO. It is unknown how much of the error at ROO is due to residual contamination by the local source discussed in section 3.5, errors in transport winds (note that simulation errors in both wind speed and direction are noted in Figure 4a), or potential errors in both the NOAA and EPA inventories. The differences in the diurnal cycle of CH₄ before and after the standard deviation filtering is applied are only ~200 ppb (Figure 10a). The maximum observed concentrations are approximately 100–150 ppb higher than those simulated, and the observed range in diurnal concentrations is close to 300 ppb, compared to a simulated range of less than 100 ppb using both emission inventories. At all locations, within a few hours before and after sunrise, the simulated CH₄ concentrations show an overall increase relative to the low concentrations simulated during the day due to accumulation in the stable nocturnal PBL, followed by a rapid “mix-out” of the CH₄ as daytime convection rapidly increases vertical mixing in late morning through the afternoon (Figure 10).

The simulated diurnal cycles at HPL and CSP using the NOAA emission inventory closely follow the observed and lie within the standard error during most hours at the two sites (Figures 10b and 10c). At HPL and CSP, the fraction of observations where modeled CH₄ ranges between 200 and 300 ppb is simulated most realistically by the STILT simulation utilizing the NOAA inventory. At CSP, analysis of the distribution of observed CH₄ concentrations to STILT simulations found that the NOAA inventory captured the relative frequency of CH₄ enhancements across the range of observations (not shown). In contrast, the STILT simulations using the EPA inventory produce almost no CH₄ enhancement above the background at CSP, with modeled CH₄ concentrations 200–400 ppb lower than observations (Figure 10c). At HPL, the STILT simulations using the NOAA inventory produced the best simulated diurnal cycle of CH₄ enhancements, with the EPA inventory STILT simulation results underestimated slightly by ~200 ppb (Figure 10b).

As discussed in sections 3.2 and 3.3, the largest source of uncertainty in the nighttime-simulated CH₄ enhancements results from potential errors in the modeled z_i , as the modeled CH₄ enhancements are

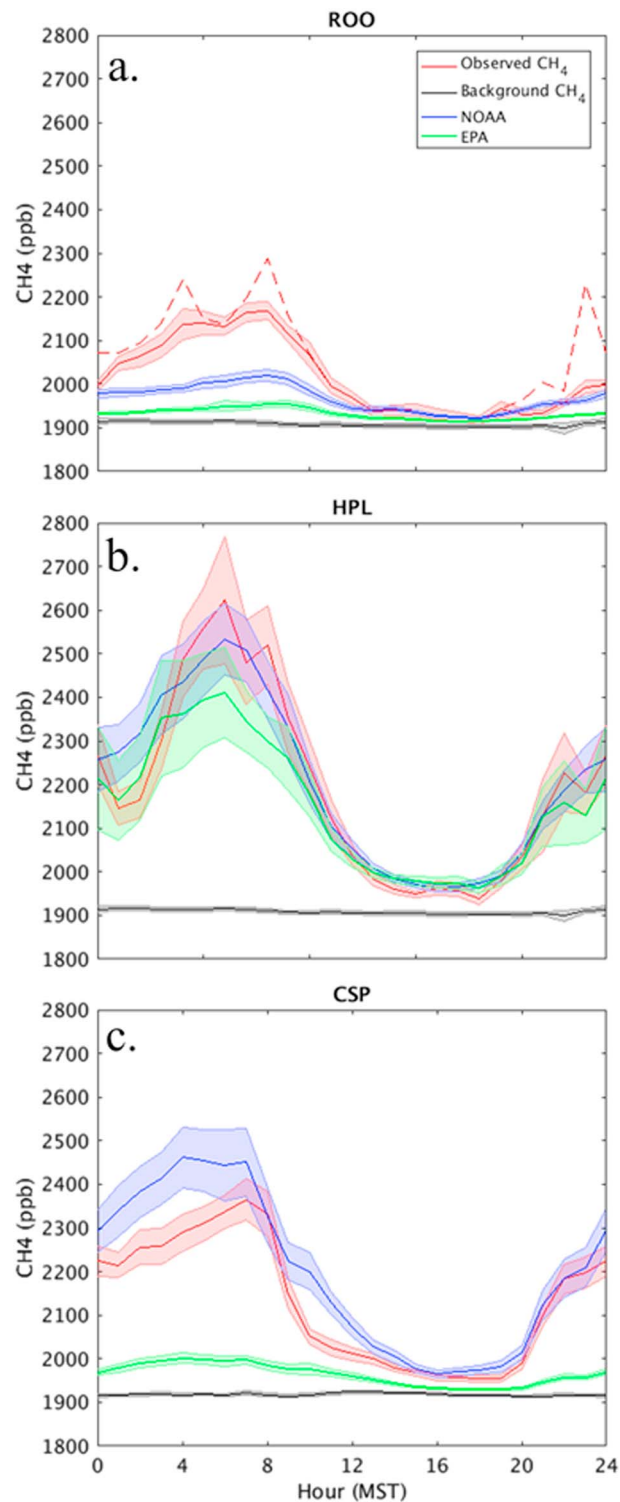


Figure 10. (a) Average CH₄ concentration (ppb) at each hour of the day (MST) during the period 19 April 2015 to 31 May 2015 on quiescent days. The red line represents observed concentrations at Roosevelt (dashed indicates unfiltered data; solid indicates filtered data). The black line represents observed concentrations at Fruitland (the background). The blue line represents simulation using the NOAA inventory at Roosevelt. The green line represents simulation using the EPA inventory at Roosevelt. The shaded area shows hourly standard errors (standard deviation of sampling distribution) for each line, colors corresponding. (b) As in Figure 10a except for Horsepool. (c) As in Figure 10a except for Castlepeak during the period 19 April 2016 to 31 May 2016.

sensitive to the magnitude of the vertical mixing and dispersion in the nocturnal boundary layer. WRF-STILT underestimates z_i at night by ~ 60 m relative to ceilometer-derived z_i . Assuming no model errors associated with variations in horizontal transport or near-surface emission rates, this would correspond to an $\sim 20\%$ change in the overall z_i and a corresponding difference in simulated CH_4 during the nocturnal period at CSP and HPL of ~ 100 ppb (Figures 10b and 10c). At CSP, the ~ 100 ppb overestimation of the WRF-STILT-simulated CH_4 enhancements at night may be partially explained by the observed model z_i bias (Figure 10c). In addition, the simulated difference in CH_4 enhancements between the NOAA and EPA inventory at CSP are several times larger (400 ppb) than the expected uncertainty in z_i , providing increased confidence in stating that the EPA CH_4 emissions inventory grossly underestimates CH_4 emissions in the CSP area. At the HPL location, simulated difference in nighttime CH_4 enhancements between the NOAA and EPA inventory are smaller (~ 100 ppb). At this location, both the EPA and NOAA inventory emission scenarios result in reasonably realistic simulations of nocturnal CH_4 enhancements.

4. Discussion

Aircraft mass balance techniques have been employed extensively to investigate emissions resulting from oil and natural gas extraction processes and have been shown to be effective in characterizing regional-scale CH_4 emissions (Barkley et al., 2017; Karion et al., 2013, 2015). However, these results generally provide Basin-wide estimates over a small sample of days when the flights take place due to difficulties inherent in the aircraft mass balance method for quantifying emissions over a longer period of time or in attributing emissions from various individual subregions. The availability of a continuous observational CH_4 data set at four sites within the Uintah Basin of eastern Utah presents the opportunity to examine CH_4 emissions in an area of active natural gas and oil industry. These observations, in combination with an atmospheric transport model, were used to test estimates from two available CH_4 emission inventories in the Uintah Basin, as well as to examine the relationship between meteorological conditions and CH_4 emissions/transport within the Basin.

Local flows and boundary layer mixing processes modulate the buildup and transport of CH_4 within the Basin and illustrate the importance of adequate meteorological model performance to simulate CH_4 within the Basin. The intrabasin transport during the spring 2015 and 2016 periods was limited, with most emissions at receptor locations originating from locations within a 30 km radius. The CH_4 emission patterns downwind of topographically confined basins such as the Uintah Basin will vary on diurnal timescales, with emissions remaining trapped in the Basin during the night but ventilating in the daytime to the free atmosphere to varying degrees during different times of the year.

This research has shown that CH_4 simulations utilizing the NOAA emission inventory (Ahmadov et al., 2015; Karion et al., 2013) performed surprisingly well when compared with observations at both CSP and HPL, despite its simplicity in spatially allocating emissions based only on well density, with no information on isolated larger emission sources that are likely important, and the inherent limitation of utilizing a “snapshot” of CH_4 emissions provided by a single flight day (Karion et al., 2013). The transport patterns and PBL characteristics were validated against meteorological observations and indicate that the uncertainty related to meteorological errors would not change the general conclusions of this study. This study provides evidence supporting basin-wide emission estimates ($55 \times 10^3 \text{ kg h}^{-1}$) found by Karion et al. (2013).

The EPA emissions inventory was found to severely underestimate CH_4 emissions from oil wells in the western Uintah Basin and to a lesser extent in the central portions of the Basin. This is not unexpected, given that EPA emission estimate uses national totals from the GHGI and then spatially allocates them based on state-level well info, while the NOAA inventory uses a basin-specific emission estimate. The EPA basin-wide methane emission rate of $31.1 \times 10^3 \text{ kg h}^{-1}$ was roughly 45% lower than that given by the NOAA emission inventory. The differences between the EPA and NOAA inventories highlight current uncertainties in estimating CH_4 emission rates, and how different methodologies impact the spatial allocation of the emission estimates. For example, the influence of a prominent processing plant, Chipeta, 10 km to the southeast of HPL, is pronounced in the facility-level accounting of emissions in the EPA inventory (Figure 3b), while its impact was not accounted for in the NOAA spatial allocation. A shortcoming of the EPA inventory is the underallocation

of CH₄ emissions in the region of oil wells located near CSP (in the southwest portion of the Basin), which is evident in the comparison of observed to simulated CH₄ concentrations at that site. Future work will seek to answer whether the observational and modeling approaches in a single region presented in this study can be used to inform spatially variable leak rates in national inventories. A key uncertainty we hope to address in future work is why the EPA inventory fails to capture most of the emission locations in the oil and gas region near CSP.

The CH₄ simulations utilizing both the NOAA and EPA emission inventories underestimate nighttime and morning CH₄ concentrations at ROO. Future research will seek to determine the reason for the underestimation at this location. Current hypotheses for this underestimate include emissions from local sources within several kilometers of the site that are not included in the inventory (e.g., local livestock and oil wells), residual contamination despite attempts to filter emissions from a nearby gas well in the observed CH₄ data (section 3.5), or meteorological transport errors. The aircraft observations from which the NOAA inventory was derived were focused on the eastern portion of the Uintah Basin but spatially allocated over the entire Basin. Hence, emission estimates in the western portion of the Basin may not be accurately represented (Ahmadov et al., 2015). The NOAA inventory approach is also limited in that it does not account for superemitters, or variations in CH₄ based on well age, type, or other factors. A recent study found that several of the well pads with the highest total mass of methane emitted as a fraction of gross methane produced were oil wells in the Uintah Basin (Robertson et al., 2017). The inability of either emission inventory to replicate the diurnal trend of CH₄ at ROO suggests that an improvement in estimated emission rates is needed in this region of the basin, the veracity of which could be tested with the technique outlined in this study.

Recent research has found that CH₄ emissions in oil and gas producing basins may vary on diurnal time-scales, driven by temporally dependent drivers such as midday routine manual liquid unloading at shale gas wells (Schwietzke et al., 2017). The NOAA inventory utilized in this study assumed constant emission rates during both day and night, and utilized data from a single daytime mass balance flight conducted over the Uintah Basin to constrain the emission estimates. The relatively good agreement of the CH₄ diurnal modeling results at the CSP and HPL sites utilizing the NOAA inventory derived from a single daytime flight and temporally allocated with constant 24 h emission rates suggests that conducting multiple flights at different times of day may not be needed to quantify Basin-wide emission rates. Future research will extend the modeling framework to a longer period and over different seasons, giving additional insight into the robustness and representativeness of the midday aircraft mass balance approach.

The CH₄ observational data set we have collected at 10 s intervals in the Basin starting in January 2015 is unique for several reasons. First, none of the previously mentioned large production regions in the U.S. are geographically situated in a deeply confined Basin where exchange between the boundary layer and free atmosphere is constrained for up to several weeks each winter season. Future work will leverage this fact and investigate emission signals at different time scales. Synthesizing all available data presents an opportunity to examine potential variations in CH₄ emissions on seasonal and multiyear time scales not readily discerned by short-term aircraft studies. Natural gas has great potential to be a “bridge fuel” between our current carbon intensive global environment and a greener, decarbonized energy system. However, a better understanding of greenhouse gas leak rates currently available from national inventories such as the EPA is needed to inform policy aimed at mitigating production leakage rates.

Large leakage events such as the failure of a natural gas storage facility in Aliso Canyon, California, attracted significant attention, which “temporarily created the largest known anthropogenic point source of CH₄ in the U.S.” (roughly $60 \times 10^3 \text{ kg h}^{-1}$) between October 2015 and February 2016 (Conley et al., 2016). In contrast, the continual leakage of CH₄ from oil and gas production facilities spread out over a much broader region emits CH₄ at rates (when aggregated at the basin level) comparable to the Aliso Canyon storage facility failure in each of the several oil and gas production regions across the U.S. (e.g., Barnett, Haynesville, and Marcellus). This study provides evidence that emissions from the Uintah Basin are likewise comparably large. However, due to the lower natural gas production amounts in the Uintah Basin relative to the aforementioned regions, the fact that our study found similar Basin-wide emission rates with other regions lends further support to the conclusion from Karion et al. (2013) that the CH₄ leak rates in the Uintah Basin are among the highest in the United States.

Acknowledgments

This study was performed with the support of NOAA Climate Program Office's Atmospheric Chemistry, Carbon Cycle, and Climate program award NA14OAR4310138. We are thankful to Scot Miller and two other reviewers whose comments greatly improved this manuscript. We would like to gratefully acknowledge Seth Lyman at Utah State University for providing expert guidance as well as observation sites and meteorological and other data in the Uintah Basin. Helpful discussions with Anna Karion are gratefully acknowledged. We thank Ravan Ahmadov for providing the NOAA emission inventory. Luke Leclair-Marzolf and Brian Blalock contributed to the meteorological analysis. Brian Speer and Jay Morris from the Utah Department of Environmental Quality, Division of Air Quality, assisted in providing and operating an IR camera. Real-time and historic measurements from all sites presented in this study can be viewed at <http://air.utah.edu>. The observational and model data used in this study are available at http://lair.utah.edu/Data/Foster_JGR_2017/. The entire CH₄ data set collected since 2015 will be archived for use by the scientific community at a formal permanent repository within the next year.

References

- Ahmadov, R., McKeen, S., Trainer, M., Banta, R., Brewer, A., Brown, S., ... Zamora, R. (2015). Understanding high wintertime ozone pollution events in an oil- and natural gas-producing region of the western US. *Atmospheric Chemistry and Physics*, *15*(1), 411–429. <https://doi.org/10.5194/acp-15-411-2015>
- Bar-Ilan, A., Grant, J., Parikh, R., Morris, R., Sgamma, K., Moore, T., & Gribovicz, L. (2008). A comprehensive emissions inventory of upstream oil and gas activities in the Rocky Mountain states. *Environmental International Corporation*, 1–35.
- Barkley, Z. R., Lauvaux, T., Davis, K. J., Deng, A., Cao, Y., Sweeney, C., ... Maasakkers, J. D. (2017). Quantifying methane emissions from natural gas production in northeastern Pennsylvania. *Atmospheric Chemistry and Physics Discussions*, 1–53. <https://doi.org/10.5194/acp-2017-200>
- Benjamin, S. G., Weygandt, S. S., Brown, J. M., Hu, M., Alexander, C. R., Smirnova, T. G., ... Manikin, G. S. (2016). A North American hourly assimilation and model forecast cycle: The rapid refresh. *Monthly Weather Review*, *144*(4), 1669–1694. <https://doi.org/10.1175/MWR-D-15-0242.1>
- Blaylock, B. K., Horel, J. D., & Crosman, E. T. (2017). Impact of lake breezes on summer ozone concentrations in the Salt Lake valley. *Journal of Applied Meteorology and Climatology*, *56*(2), 353–370. <https://doi.org/10.1175/JAMC-D-16-0216.1>
- Brandt, A. R., Heath, G. A., Kort, E. A., O'Sullivan, F., Petron, G., Jordaan, S. M., ... Harriss, R. (2014). Methane leaks from North American natural gas systems. *Science*, *343*(6172), 733–735. <https://doi.org/10.1126/science.1247045>
- Conley, S., Franco, G., Faloon, I., Blake, D. R., Peischl, J., & Ryerson, T. B. (2016). Methane emissions from the 2015 Aliso Canyon blowout in Los Angeles, CA. *Science*, *351*(6279), 1317–1320. <https://doi.org/10.1126/science.aaf2348>
- Crosman, E. T., & Horel, J. D. (2017). Large-eddy simulations of a Salt Lake Valley cold-air pool. *Atmospheric Research*, *193*, 10–25. <https://doi.org/10.1016/j.atmosres.2017.04.010>
- Desai, M., & Harvey, R. P. (2017). Inventory of U.S. greenhouse gas emissions and sinks: 1990–2015. *Federal Register*, 1–633.
- Edwards, P. M., Brown, S. S., Roberts, J. M., Ahmadov, R., Banta, R. M., deGouw, J. A., ... Zamora, R. (2014). High winter ozone pollution from carbonyl photolysis in an oil and gas basin. *Nature*, *514*(7522), 351–354. <https://doi.org/10.1038/nature13767>
- Foster, C. S., Crosman, E. T., & Horel, J. D. (2017). Simulations of a cold-air pool in Utah's Salt Lake Valley: Sensitivity to land use and snow cover. *Boundary-Layer Meteorology*, *164*(1), 63–87. <https://doi.org/10.1007/s10546-017-0240-7>
- Gerbig, C., Körner, S., & Lin, J. C. (2008). Vertical mixing in atmospheric tracer transport models: Error characterization and propagation. *Atmospheric Chemistry and Physics*, *8*, 591–602. <https://doi.org/10.5194/acp-8-591-2008>
- Karion, A., Sweeney, C., Kort, E. A., Shepson, P. B., Brewer, A., Cambaliza, M., ... Tans, P. (2015). Aircraft-based estimate of Total methane emissions from the Barnett Shale Region. *Environmental Science & Technology*, *49*(13), 8124–8131. <https://doi.org/10.1021/acs.est.5b00217>
- Karion, A., Sweeney, C., Pétron, G., Frost, G., Michael Hardesty, R., Kofler, J., ... Conley, S. (2013). Methane emissions estimate from airborne measurements over a western United States natural gas field. *Geophysical Research Letters*, *40*, 4393–4397. <https://doi.org/10.1002/grl.50811>
- Kotthaus, S., O'Connor, E., Munkel, C., Charlton-Perez, C., Haeffelin, M., Gabey, A. M., & Grimmond, C. S. B. (2016). Recommendations for processing atmospheric attenuated backscatter profiles from Vaisala CL31 ceilometers. *Atmospheric Measurement Techniques*, *9*(8), 3769–3791. <https://doi.org/10.5194/amt-9-3769-2016>
- Lin, J. C., Gerbig, C., Wofsy, S. C., Andrews, A. E., Daube, B. C., Davis, K. J., & Grainger, C. A. (2003). A near-field tool for simulating the upstream influence of atmospheric observations: The Stochastic Time-Inverted Lagrangian Transport (STILT) model. *Journal of Geophysical Research*, *108*(D16), 4493. <https://doi.org/10.1029/2002JD003161>
- Lyman, S., & Tran, T. (2015). Inversion structure and winter ozone distribution in the Uintah Basin, Utah, U.S.A. *Atmospheric Environment*, *123*, 156–165. <https://doi.org/10.1016/j.atmosenv.2015.10.067>
- Lyon, D. R., Zavala-Araiza, D., Alvarez, R. A., Harriss, R., Palacios, V., Lan, X., ... Hamburg, S. P. (2015). Constructing a spatially resolved methane emission inventory for the Barnett Shale Region. *Environmental Science & Technology*, *49*(13), 8147–8157. <https://doi.org/10.1021/es506359c>
- Maasakkers, J. D., Jacob, D. J., Sulprizio, M. P., Turner, A. J., Weitz, M., Wirth, T., ... Fischer, M. L. (2016). Gridded national inventory of U.S. methane emissions. *Environmental Science & Technology*, *50*(23), 13,123–13,133. <https://doi.org/10.1021/acs.est.6b02878>
- Mallia, D. V., Lin, J. C., Urbanski, S., Ehleringer, J., & Nehrkorn, T. (2015). Impacts of upwind wildfire emissions on CO, CO₂, and PM_{2.5} concentrations in Salt Lake City, Utah. *Journal of Geophysical Research: Atmospheres*, *120*, 147–166. <https://doi.org/10.1002/2014JD022472>
- Mayfield, E. N., Robinson, A. L., & Cohon, J. L. (2017). System-wide and superemitter policy options for the abatement of methane emissions from the U.S. natural gas system. *Environmental Science & Technology*, *51*(9), 4772–4780. <https://doi.org/10.1021/acs.est.6b05052>
- Miller, S. M., Wofsy, S. C., Michalak, A. M., Kort, E. A., Andrews, A. E., Biraud, S. C., ... Sweeney, C. (2013). Anthropogenic emissions of methane in the United States. *Philippines of National Academy Sciences of United States of America*, *110*(50), 20,018–20,022. <https://doi.org/10.1073/pnas.1314392110>
- Neemann, E. M., Crosman, E. T., Horel, J. D., & Avey, L. (2015). Simulations of a cold-air pool associated with elevated wintertime ozone in the Uintah Basin, Utah. *Atmospheric Chemistry and Physics*, *15*(1), 135–151. <https://doi.org/10.5194/acp-15-135-2015>
- Nehrkorn, T., Eluszkiewicz, J., Wofsy, S. C., Lin, J. C., Gerbig, C., Longo, M., & Freitas, S. (2010). Coupled weather research and forecasting-stochastic time-inverted lagrangian transport (WRF-STILT) model. *Meteorology and Atmospheric Physics*, *107*, 51–64. <https://doi.org/10.1007/s00703-010-0068-x>
- NOAA (2014). Studying the atmospheric effects of changing energy use in the U. S. at the Nexus of air quality and climate change. *Shale Oil Natural Gas Nexus*, 1–16.
- Oltmans, S. J., Karion, A., Schnell, R. C., Pétron, G., Helmig, D., Montzka, S. A., ... Sweeney, C. (2016). O₃, CH₄, CO₂, CO, NO₂ and NMHC aircraft measurements in the Uinta Basin oil and gas region under low and high ozone conditions in winter 2012 and 2013. *Elementa: Science of the Anthropocene*, *4*(132), 1–12. <https://doi.org/10.12952/journal.elementa.000132>
- Peischl, J., Karion, A., Sweeney, C., Kort, E. A., Smith, M. L., Brandt, A. R., ... Ryerson, T. B. (2016). Locating and quantifying greenhouse gas emissions at a geological CO₂ storage site using atmospheric modeling and measurements. *Journal of Geophysical Research: Atmospheres*, *121*, 6101–6111. <https://doi.org/10.1002/2015JD024631>
- Peischl, J., Ryerson, T. B., Aikin, K. C., de Gouw, J. A., Gilman, J. B., Holloway, J. S., ... Parrish, D. D. (2015). Quantifying atmospheric methane emissions from the Haynesville, Fayetteville, and northeastern Marcellus shale gas production regions. *Journal of Geophysical Research: Atmospheres*, *120*, 2119–2139. <https://doi.org/10.1002/2014JD022697>
- Petron, G., Karion, A., Sweeney, C., Miller, B. R., Montzka, S. A., Frost, G. J., ... Schnell, R. (2014). A new look at methane and nonmethane hydrocarbon emissions from oil and natural gas operations in the Colorado Denver-Julesburg Basin. *Journal of Geophysical Research: Atmospheres*, *119*, 6836–6852. <https://doi.org/10.1002/2013JD021272>

- Ravikumar, A. P., & Brandt, A. R. (2017). Designing better methane mitigation policies: The challenge of distributed small sources in the natural gas sector. *Environmental Research Letters*, 12(4), 044023. <https://doi.org/10.1088/1748-9326/aa6791>
- Robertson, A. M., Edie, R., Snare, D., Soltis, J., Field, R. A., Burkhart, M. D., ... Murphy, S. M. (2017). Variation in methane emission rates from well pads in four oil and gas basins with contrasting production volumes and compositions. *Environmental Science & Technology*, 51(15), 8832–8840. <https://doi.org/10.1021/acs.est.7b00571>
- Rozell, D. J., & Reaven, S. J. (2012). Water pollution risk associated with natural gas extraction from the Marcellus shale. *Risk Analysis*, 32, 1382–1393. <https://doi.org/10.1111/j.1539-6924.2011.01757.x>
- Sahoo, P. K., Soltani, S., & Wong, A. K. C. (1988). A survey of thresholding techniques. *Computer Vision, Graphics, and Image Processing*, 41(2), 233–260. [https://doi.org/10.1016/0734-189X\(88\)90022-9](https://doi.org/10.1016/0734-189X(88)90022-9)
- Schnell, R. C., Johnson, B. J., Oltmans, S. J., Cullis, P., Sterling, C., Hall, E., ... Park, J. H. (2016). Quantifying wintertime boundary layer ozone production from frequent profile measurements in the Uinta Basin, UT, oil and gas region. *Journal of Geophysical Research: Atmospheres*, 121, 11,038–11,054. <https://doi.org/10.1002/2016JD025130>
- Schnell, R. C., Oltmans, S. J., Neely, R. R., Endres, M. S., Molenaar, J. V., & White, A. B. (2009). Rapid photochemical production of ozone at high concentrations in a rural site during winter. *Nature Geoscience*, 2, 120–122. <https://doi.org/10.1038/ngeo415>
- Schwietzke, S., Pétron, G., Conley, S., Pickering, C., Mielke-Maday, I., Dlugokencky, E. J., ... Schnell, R. C. (2017). Improved mechanistic understanding of natural gas methane emissions from spatially-resolved aircraft measurements. *Environmental Science & Technology*, 51(12), 7286–7294. <https://doi.org/10.1021/acs.est.7b01810>
- Seibert, P., Beyrich, F., Gryning, S.-E., Joffre, S., Rasmussen, A., & Tercier, P. (2000). Review and intercomparison of operational methods for the determination of the mixing height. *Atmospheric Environment*, 34(7), 1001–1027. [https://doi.org/10.1016/S1352-2310\(99\)00349-0](https://doi.org/10.1016/S1352-2310(99)00349-0)
- Skamarock, W. C., Klemp, J. B., Dudhi, J., Gill, D. O., Barker, D. M., Duda, M. G., ... Powers, J. G. (2008). A description of the Advanced Research WRF version 3 (NCAR Tech. Rep., pp. 1–113). <https://doi.org/10.5065/D6DZ069T>
- Smith, M. L., Gvakharia, A., Kort, E. A., Sweeney, C., Conley, S. A., Faloon, I., ... Wolter, S. (2017). Airborne quantification of methane emissions over the four corners region. *Environmental Science & Technology*, 51(10), 5832–5837. <https://doi.org/10.1021/acs.est.6b06107>
- Subramanian, R., Williams, L. L., Vaughn, T. L., Zimmerle, D., Roscioli, J. R., Herndon, S. C., ... Robinson, A. L. (2015). Methane emissions from natural gas compressor stations in the transmission and storage sector: Measurements and comparisons with the EPA greenhouse gas reporting program protocol. *Environmental Science & Technology*, 49(5), 3252–3261. <https://doi.org/10.1021/es5060258>
- Turner, A. J., Jacob, D. J., Benmergui, J., Wofsy, S. C., Maasakkers, J. D., Butz, A., ... Biraud, S. C. (2016). A large increase in U.S. methane emissions over the past decade inferred from satellite data and surface observations. *Geophysical Research Letters*, 43(5), 2218–2224. <https://doi.org/10.1002/2016GL067987>
- Vogelezang, D. H. P., & Holtslag, A. A. M. (1996). Evaluation and model impacts of alternative boundary-layer height formulations. *Boundary-Layer Meteorology*, 81(3-4), 245–269. <https://doi.org/10.1007/BF02430331>
- Wang, Q., Chen, X., Jha, A. N., & Rogers, H. (2014). Natural gas from shale formation—The evolution, evidences and challenges of shale gas revolution in United States. *Renewable and Sustainable Energy Reviews*, 30, 1–28. <https://doi.org/10.1016/j.rser.2013.08.065>
- Ware, J., Kort, E. A., DeCola, P., & Duren, R. (2016). Aerosol lidar observations of atmospheric mixing in Los Angeles: Climatology and implications for greenhouse gas observations. *Journal of Geophysical Research: Atmospheres*, 121, 9862–9878. <https://doi.org/10.1002/2016JD024953>
- Young, J. S., & Whiteman, C. D. (2015). Laser ceilometer investigation of persistent wintertime cold-air pools in Utah's Salt Lake Valley. *Journal of Applied Meteorology and Climatology*, 54(4), 752–765. <https://doi.org/10.1175/JAMC-D-14-0115.1>
- Yuan, B., Liggio, J., Wentzell, J., Li, S. M., Stark, H., Roberts, J. M., ... de Gouw, J. A. (2016). Secondary formation of nitrated phenols: Insights from observations during the Uintah Basin Winter Ozone Study (UBWOS) 2014. *Atmospheric Chemistry and Physics*, 16(4), 2139–2153. <https://doi.org/10.5194/acp-16-2139-2016>
- Zatko, M., Erbland, J., Savarino, J., Geng, L., Easley, L., Schauer, A., ... Alexander, B. (2016). The magnitude of the snow-sourced reactive nitrogen flux to the boundary layer in the Uintah Basin, Utah, USA. *Atmospheric Chemistry and Physics*, 16(21), 13,837–13,851. <https://doi.org/10.5194/acp-16-13837-2016>